The Astrophysical Journal, 573:157–167, 2002 July 1
© 2002. The American Astronomical Society. All rights reserved. Printed in U.S.A.

CHANDRA DISCOVERY OF A TREE IN THE X-RAY FOREST TOWARD PKS 2155−304: THE LOCAL FILAMENT?

Fabrizio Nicastro,[1] Andreas Zezas,[1] Jeremy Drake,[1] Martin Elvis,[1] Fabrizio Fiore,[2] Antonella Fruscione,[1] Massimo Marengo,[1] Smita Mathur,[3] and Stefano Bianchi[4]

Received 2001 September 4; accepted 2002 March 1

ABSTRACT

We present the first X-ray detection of resonant absorption from warm/hot local gas either in our Galaxy, or in the intergalactic space surrounding our Galaxy, along the line of sight toward the blazar PKS 2155−304. The *Chandra* HRCS/LETG spectrum of this $z = 0.116$ source clearly shows, at $\geq 5\,\sigma$ level, unresolved (FWHM $\leq$ 800 km s^{-1} at a 2 σ confidence level) O VII Kα and Ne IX Kα resonant absorption lines at $21.603^{+0.014}_{-0.024}$ and $13.448^{+0.022}_{-0.024}$ Å (i.e., $cz = 14^{+190}_{-330}$ km s^{-1} in the rest frame, from the O VII Kα line). O VIII Kα and O VII Kβ from the same system are also detected at a lower significance level (i.e., $\sim 3\,\sigma$), while upper limits are set on O VIII Kβ, Ne X Kα, and Ne IX Kβ. The *Far Ultraviolet Spectroscopic Explorer* spectrum of this source shows complex O VI $2s \rightarrow 2p$ absorption at the same redshift as the X-ray system, made by at least two components: one relatively narrow (FWHM $= 106 \pm 9$ km s^{-1}) and slightly redshifted ($cz = 36 \pm 6$ km s^{-1}), and one broader (FWHM $= 158 \pm 26$ km s^{-1}) and blueshifted ($cz = -135 \pm 14$ km s^{-1}). We demonstrate that the physical states of the UV and X-ray absorbers are hard to reconcile with a single, purely collisionally ionized, equilibrium plasma. We propose instead that the X-ray and at least the broader and blueshifted UV absorber are produced in a low-density intergalactic plasma, collapsing toward our Galaxy, consistent with the predictions of a warm-hot intergalactic medium from numerical simulations. We find that any reasonable solution requires overabundance of Ne compared to O by a factor of $\sim$2, with respect to the solar value. We propose several scenarios to account for this observation.

Subject headings: Galaxy: halo — intergalactic medium — quasars: absorption lines — X-rays: ISM

1. INTRODUCTION

The majority of the total baryonic matter in the local ($z \lesssim 1$) universe is predicted to be concentrated in highly ionized gas. Structures that are already virialized contain warm (10^5–10^6 K) or hot (10^7 K) gas (the dense interstellar medium [ISM] of galaxies, and the intracluster medium [ICM] of clusters of galaxies). The greater amount of baryonic matter is predicted to lie in, as yet unvirialized, matter in the form of a tenuous warm-hot intergalactic medium (WHIM; Hellsten, Gnedin, & Miralda-Escudé 1998). The detection and study of these components is needed for the proper understanding of large- and small-scale structures in the universe. However, while X-ray emission from the virialized density peaks of the ICM and ISM has been detected and intensively studied in X-rays, the predicted highly ionized gas in the WHIM has been poorly studied so far because of instrumental limitations. The low density of the WHIM leads to low emissivity so that studies of the WHIM in emission are a formidable challenge. However, absorption depends only on the total column density of the medium, not on density, and background light sources in the form of quasars (Aldcroft et al. 1994) and gamma-ray bursts (Fiore et al. 2000) are readily available. A few high-ionization transitions, notably O VI λ1031.93, lie in the UV, but the most prominent ions (C VI, O VII, O VIII, Ne IX) have their strongest transitions in the soft X-ray band (10–40 Å) for a wide range of temperatures (10^5–$10^{6.5}$ K; Nicastro et al. 1999b), which should give rise to an "X-ray forest" of absorption lines (e.g., Perna & Loeb 1998; Fang & Canizares 2000). The advent of high-resolution ($R \sim 1000$) soft X-ray spectroscopy with *Chandra* and *XMM-Newton* allows sensitive studies of the WHIM possible.

Interstellar O VI was first detected in the UV with the *Copernicus* satellite (Jenkins 1978a, 1978b; York 1977), but only recently has data from the *Far Ultraviolet Spectroscopic Explorer* (*FUSE*) satellite shown the presence of extragalactic O VI intervening absorpion (e.g., Tripp et al. 2001; Sembach et al. 2000).

In this paper we present the first X-ray detection of highly ionized absorption along the line of sight toward the blazar PKS 2155−304, with the *Chandra* High Resolution Camera Spectrometer/Low Energy Transmission Grating (HRCS/LETG; Brinkman et al. 2000). We argue that the physical and dynamical conditions implied by these lines require an extragalactic, low-density origin. Hence, these lines are the first detection of the X-ray forest.

2. SPECTRAL FITTING

The bright $z = 0.116$ blazar PKS 2155−304 (Falomo, Pesce, & Treves 1993) is a calibration source for both the high-energy and low-energy resolution gratings of *Chandra* and has been observed several times with all the possible grating-detector configurations. The longest of these observation lasted $\sim$64.7 ks, for a total net good-time exposure of 62.7 ks, and was performed with the HRCS/LETG configu-

[1] Harvard-Smithsonian Center for Astrophysics, 60 Garden Street, Cambridge, MA 02138.
[2] Osservatorio Astronomico di Roma, Via Frascati 33, I-00040 Monte Porzio Catone, Rome, Italy.
[3] Astronomy Department, Ohio State University, Columbus, OH 43210.
[4] Dipartimento di Fisica, Universitá degli Studi Roma Tre, Via della Vasca Navale 84, I-00146 Rome, Italy.

ration on 1999 December 25. In the public *Chandra* data archive[5] we found two more HRCS/LETG observations of this source, performed on 2000 May 31 and 2001 April 6, with net exposures of 25.8 and 26.6 ks, respectively.

We retrieved the primary and secondary data products (G. Fabbiano et al. 2002, in preparation) of these three *Chandra* HRCS/LETG observations of PKS 2155−304 and reprocessed their event files with the CIAO (M. Elvis et al. 2002, in preparation) software (version 2.1.3), using the most up-to-date calibration files as of 2001 August (CALDB version 6.2) to extract source and background spectra and corresponding first-order anciliary response files (ARFs) and redistribution matrices (RMFs) according to the on-line data analysis "threads" provided by the *Chandra* X-Ray Center (CXC).[6]

During the long 1999 December observation the source was at the particularly high-flux level of 21 mcrab, with a 0.3–6 keV flux of $F_{2-40\,\text{Å}} = 4.2 \times 10^{-10}$ ergs s^{-1} cm^{-2}. In both the subsequent HRCS/LETG observations, instead, the flux level of PKS 2155−304 was more normal at about 6 mcrab in the 0.3–6 keV band. However, despite the large change in flux, the spectral shape of the underlying 0.3–6 keV continuum did not change significantly between or during the three observations (using simple power-law continuum models, we measured variations in the spectral slope to be less than $\Delta\Gamma = 0.1$ at 90% confidence level). To increase the signal-to-noise ratio of our data, we then coadded the three HRCS/LETG spectra and averaged the corresponding ARFs, weighting them by the respective exposure times. The result (Fig. 1a) is one of the highest quality *Chandra* grating spectra so far for an extragalactic source, with some 600 counts, or a signal-to-noise ratio of about 25, per resolution element ($R \sim 450$, FWHM $\simeq$ 660 km s^{-1} at 20 Å) in the continuum, over the entire 10–25 Å wavelength (∼0.5–1.2 keV) range.

To ensure a self-consistent analysis, and because of the ∼30 times higher spectral resolution provided, we also retrieved the *FUSE* (Moos et al. 2000) data of PKS 2155−304 from the *FUSE* public archive, extracted the fluxed spectrum, and analyzed the wavelength range around O VI (1027–1035 Å) and O I (1037–1040 Å) to obtain independent estimates of the positions, widths, and equivalent widths of the local O VI $2s \rightarrow 2p$ ($\lambda = 1031.9261$) and O I $3s \rightarrow 3p$ ($\lambda = 1039.23$) components, recently discovered and published by Savage et al. (2000) and Sembach et al. (2000). The *FUSE* observation was taken with the LWRS aperture ($30'' \times 30''$) with a total exposure time of 38.6 ks and covers the entire 980–1180 Å range. We used data from the LiF mirror and the A1 detector segment, which have optimal efficiency in the waveband around the O VI line. The data were calibrated and cleaned following the procedures presented in the *FUSE* Data Analysis Cookbook version 1.0.[7] The resolution of the final data is ∼20 km s^{-1}.

We performed simultaneous spectral fitting of both the fluxed *FUSE* data and the responses-folded *Chandra* HRCS/LETG data, using the SHERPA (A. Siemiginowska et al. 2002, in preparation) package for spectral fitting in CIAO. In the following two sections we summarize our results.

[5] See http://asc.harvard.edu/cda/.

[6] See http://asc.harvard.edu/ciao/documents_threads.html.

[7] See http://fuse.pha.jhu.edu/analysis/cookbook.html.

2.1. *X-Ray Spectral Fitting*

For sources of a few millicrab the inherent order confusion problem of the *Chandra* HRCS/LETG (Brinkman et al. 2000) is important only at $\lambda \gtrsim 25$ Å. Furthermore, narrow features, such as absorption lines, are not in any case seriously affected. So we limited our spectral analysis to the shorter wavelengths of 11–24 Å (∼0.5–1.2 keV) range, allowing us to use only the first-order RMFs and ARFs to fit our spectra. Errors throughout the paper are quoted at a 90% confidence level for one interesting parameter.

To model the 11–24 Å portions of the continuum of PKS 2155−304, we used a power law attenuated by an equivalent hydrogen column density of $N_{\rm H} = 1.65 \times 10^{20}$ cm^{-2} neutral gas to account for the measured Galactic absorption from cold gas along the line of sight to this source (Dickey & Lockman 1990).[8] The model used for the neutral absorber includes only photoelectric edges by neutral elements and so does not account for resonant absorption lines from the same elements. We obtained a statistically acceptable fit with a power-law photon index of $\Gamma = 2.42 \pm 0.02$, consistent with previous results (e.g., Kataoka et al. 2000).

The residuals to this fit clearly show (at a significance level greater than 8 σ) two strong and unresolved (see § 3.1) features in absorption (Figs. 1*b* and 1*d*), at wavelengths consistent with the O VII Kα and the Ne IX Kα resonant lines at zero velocity, plus a third intense O I 1s→2p resonant absorption line from gaseous O I (Fig. 1*c*). Negative residuals are also present at the energy of the instrumental resonant molecular O I absorption line (Fig. 1*c*). The residuals around the expected O VIII Kα and the O VII Kβ rest-frame wavelengths also show absorption features at a lower (∼3 σ) significance level (Fig. 1*e*; see § 3.1). We added six negative gaussians to our continuum model and refitted the data, leaving the positions and the total flux of all the gaussians free to vary independently, but linking all the widths (in units of km s^{-1}) of the high-ionization resonance lines from O and Ne.

The best-fitting line parameters values are listed in Table 1, along with the derived ion column densities for all the atomic transitions.[9] We also include in Table 1 the 2 σ upper limits on the equivalent widths of the two lines of Ne X Kα and Ne IX Kβ, which we derived by adding two more gaussians to our model, freezing their positions to the rest-frame wavelengths of these transitions and calculating the errors on the lines' normalizations.

The strong solid state instrumental O I line at ∼23.3 Å (Figs. 1*a* and 1*c*) is only partly accounted for by the current effective area model (Fig. 1*c*, *dashed curve*; see also Table 1) and is easily separated by the HRCS/LETG from the gas phase O I 1s→2p resonant transition at λ(O I) = 23.489 Å

[8] Due to the high degree of saturation of the Galactic disk $N_{\rm H}$, the local damped Lyα absorption line in the *HST*-STIS spectrum of PKS 2155−304 cannot provide a better estimate of the Galactic column of neutral H along this line of sight.

[9] We use the line response function of the *Chandra* HRCS/LETH to convolve all components of our model through the instrument response. This implies that all gaussians in the model with width smaller than the line response FWHM are automatically broadened at the instrument resolution in the fit. Single lines with intrinsic FWHM smaller than the instrument resolution, or multiple components each narrower than the instrument resolution divided by the number of components, are then, by definition, unresolved in these fits, and only an upper limit can be set on their width, as shown in Table 1.

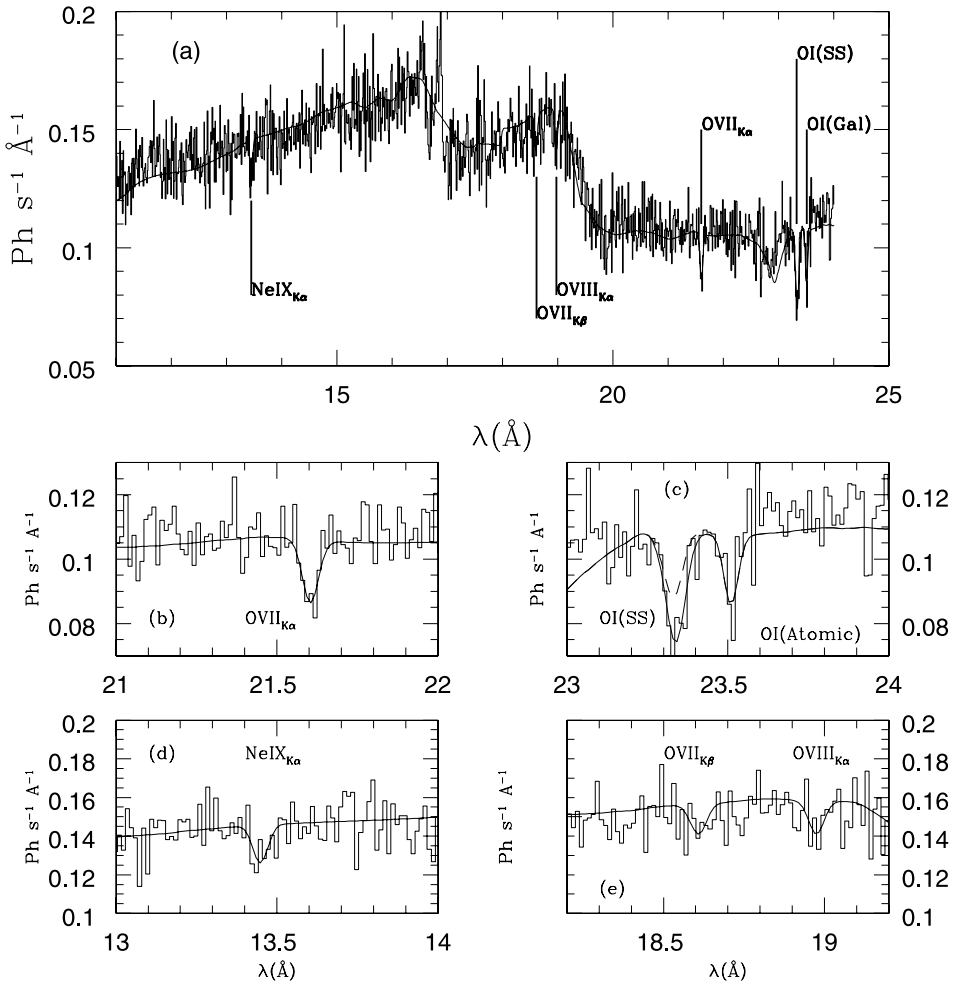

FIG. 1.— (*a*) X-ray 11-24 Å unbinned ($\Delta\lambda = 12.5$ mÅ) HRCS/LETG spectrum of PKS 2155−304. The folded best-fitting model (power law plus Galactic absorption, plus six absorption lines) is shown as a solid line. The strongest absorption lines are identified. Note that the effective area of the HRCS/LETG has not been corrected for in this plot, in order to show the strong, but large-scale, instrumental features. The fitted power law follows these peaks and dips closely. (*b–e*) Blow-ups of four portions of the spectrum in (*a*). (*b*) O VII Kα; (*c*) atomic and solid-state (i.e., molecular) O I; (*d*) Ne IX Kα; (*e*) O VII Kβ and O VIII Kα. (Note that, in the shown wavelength interval, the SHERPA fitting routine finds only the two gaussians at the positions of the O VII Kβ and O VIII Kα, although all the parameters of the gaussians are left free to vary in the fit. The negative residuals at ∼18.7 Å are narrower than the instrument resolution, and so no χ^2 local minimum can be found with a gaussian at the position of this feature.) Vertical lines indicate the rest-frame wavelengths of the transitions. The solid-state O I line in (*c*) is an effective area feature (*dashed line*).

TABLE 1

BEST-FITTING UV AND X-RAY ABSORPTION LINE PARAMETERS

Line ID	λ (Å)	cz (km s^{-1})	FWHM (km s^{-1})	EW(abs)[a] (eV)	$N_{\rm ion}$ ($\times 10^{15}$ cm^{-2})
			FUSE		
Narrow O VI $2s\rightarrow 2p$	1032.05 ± 0.02	36 ± 6	106 ± 9	$(2.1 \pm 0.2) \times 10^{-3}$	0.14 ± 0.10
Broad O VI $2s\rightarrow 2p$	1031.46 ± 0.05	-135 ± 14	158 ± 26	$(1.6 \pm 0.4) \times 10^{-3}$	0.11 ± 0.30
			Chandra		
O VII Kα	$21.603^{+0.014}_{-0.024}$	14^{+194}_{-334}	<800	$(0.31^{+0.20}_{-0.16})$	$4.0^{+2.6}_{-2.1}$
O VIII Kα	$18.973^{+0.022}_{-0.036}$	63^{+348}_{-570}	$\equiv$ FWHM(O VII Kα)	$(0.24^{+0.20}_{-0.18})$	$5.2^{+4.3}_{-3.9}$
O VII Kβ	$18.605^{+0.056}_{-0.088}$	-380^{+900}_{-1400}	$\equiv$ FWHM(O VII Kα)	$(0.22^{+0.26}_{-0.20})$	13^{+15}_{-12}
Ne IX Kα	$13.448^{+0.022}_{-0.024}$	20^{+490}_{-536}	$\equiv$ FWHM(O VII Kα)	$(0.53^{+0.36}_{-0.34})$	$6.7^{+4.6}_{-4.3}$
Ne X Kα	12.134[b]	0[b]	$\equiv$ FWHM(O VII Kα)	<0.32	<5.2
Ne IX Kβ	11.5467[b]	0[b]	$\equiv$ FWHM(O VII VII Kα)	<0.24	<20
O I ($\lambda = 23.489$[c])	$23.509^{+0.008}_{-0.018}$	-140^{+114}_{-230}	<170	$(0.25^{+0.12}_{-0.12})$	21 ± 10
O I (molecular)	$23.341^{+0.026}_{-0.018}$	N.A.	<505	$(0.30^{+0.22}_{-0.18})$	

[a] Absorption line EWs are formally negative; here we drop the sign.
[b] Frozen.
[c] Krause 1994.

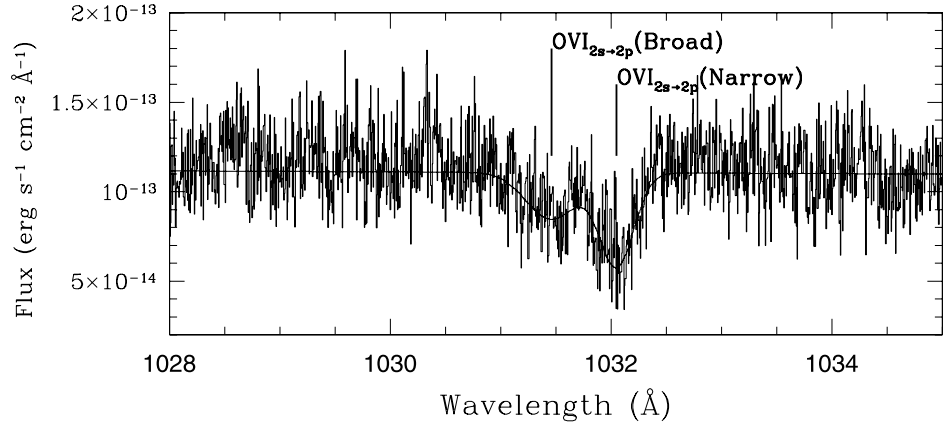

FIG. 2.—Ultraviolet 1027–1035 Å fluxed *FUSE* spectrum of PKS 2155−304, and best-fitting model

(Krause 1994), which is also clearly visible in our data (Fig. 1*c*), and will be the object of study of a forthcoming paper. Here we stress only how the intervening Galactic cold absorber is clearly distinguished from the highly ionized intervening medium seen through the He-like and H-like resonant lines from O and Ne (Table 1; see also § 3.1 for differences in the dynamics).

2.2. *UV Spectral Fitting*

We also used SHERPA to fit the 1027–1035 Å portion of the *FUSE* spectrum of PKS 2155−304 around the strongest line of the O VI $2s\rightarrow2p$ doublet, at $\lambda = 1031.9261$ Å. Residuals after a fit with a power-law continuum model, show resolved O VI $2s\rightarrow2p$ absorption in these data, with at least two components present (Fig. 2). We added two negative gaussians to our best-fit continuum model. The fit shows that one line is relatively narrow (FWHM $= 106 \pm 9$ km s^{-1}) and slightly redshifted ($cz = 36 \pm 6$ km s^{-1} in the rest frame), and the other is broader (FWHM $= 158 \pm 26$ km s^{-1}) and blueshifted ($cz = -135 \pm 14$ km s^{-1}; see Table 1). These values (and those of the equivalent widths of two lines; see Table 1), are consistent with those reported by Savage et al. (2000) and Sembach et al. (2000).

We looked for Lyα absorption associated with these two components but verified that they both would fall well within the Voigt wings of the damped Lyα because of cold absorption in our own Galaxy and so are not visible.

The *FUSE* spectrum of PKS 2155−304 also shows the presence of strong O I $3s\rightarrow3p(\lambda = 1039.23)$ absorption (see Sembach et al. 2000, Fig. 1). For this line we measure $\lambda = 1039.19 \pm 0.02$ ($cz = -11 \pm 6$ km s^{-1}) and FWHM of 47 ± 5 km s^{-1}, much narrower than the width of either of the O VI 3s→3p components.

3. ANALYSIS OF ABSORPTION LINES

3.1. *Gas Dynamics*

To intercompare the dynamics of the gas producing the detected absorption lines, Figure 3 shows their residuals, in velocity space, from the *FUSE* and *Chandra* spectra to their best-fitting continuum models. Zero velocities in this diagram correspond to the rest-frame wavelengths of the detected transitions (Verner, Verner, & Ferland 1996; Krause 1994). The spectral resolution of the HRCS/LETG ($R \sim 450$, FWHM $\simeq 660$ km s^{-1} at 20 Å) does not resolve the high-ionization X-ray absorption lines (see Table 1).

The spectral resolution of the *FUSE* spectrometer ($R \sim 15,000$, FWHM $\simeq 20$ km s^{-1} at $\sim$1000 Å) is more than 1 order of magnitude larger than that of the *Chandra* HRCS/LETG and is sufficient to resolve the O VI $2s\rightarrow2p$ absorption into at least two components (Fig. 3*a*; Table 1). The total width of the O VI $2s\rightarrow2p$ complex in the *FUSE* spectrum is FWHM $= 264 \pm 35$ km s^{-1}, fully consistent with the upper limit on the width of the high-ionization X-ray lines (Table 1). We also note that both position and width of the O I $3s\rightarrow3p(\lambda = 1039.23)$ absorption line in the *FUSE* spectrum are clearly different from widths and positions of each of the two O VI components in the same spectrum (Figs. 3*a* and 3*f*), but again fully consistent with width and position of the O I ($\lambda = 23.489$) line in the *Chandra* spectrum (Figs. 3*c* and 3*f*; Table 1).

We then conclude that (1) the high-ionization lines in both the UV and X-rays are likely to be produced by gas with similar dynamical properties and broad range of dispersion velocities (from the UV profile), while (2) the low-ionization atomic O I lines (in both *FUSE* and *Chandra*) are produced by a slow-moving cloud of cold gas, with relatively low internal dispersion velocity and so differs dramatically in both physical and dynamical properties from the high-ionization gas. In the following we discuss only the highly ionized component.

3.2. *Curve of Growth Analysis*

Absorption line equivalent widths (EWs) and their ratios can, in principle, provide invaluable information on the physical state of the gas and allow one to distinguish between quite different scenarios. However, these diagnostics can only be applied to unsaturated lines. Fortunately, the UV O VI $2s\rightarrow2p$ lines are clearly not saturated, since the ratio between the EWs of the doublet ($\lambda_1 = 1031.9261$ Å and $\lambda_2 = 1037.6167$ Å) is fully consistent with the oscillator strengths (OSs) ratio of 2 (Savage et al. 2000). For the X-ray lines of O VII, O VIII, and Ne IX, in principle, one could compare the EWs of the corresponding Kα and Kβ lines. However, the errors on the EWs of the Kβ lines from these ions are too large. An alternative approach uses the curve of growth (COG; e.g., Spitzer 1978), computed for a given Doppler parameter, to see whether each line falls on the linear branch of the COG. We ran our model for resonant

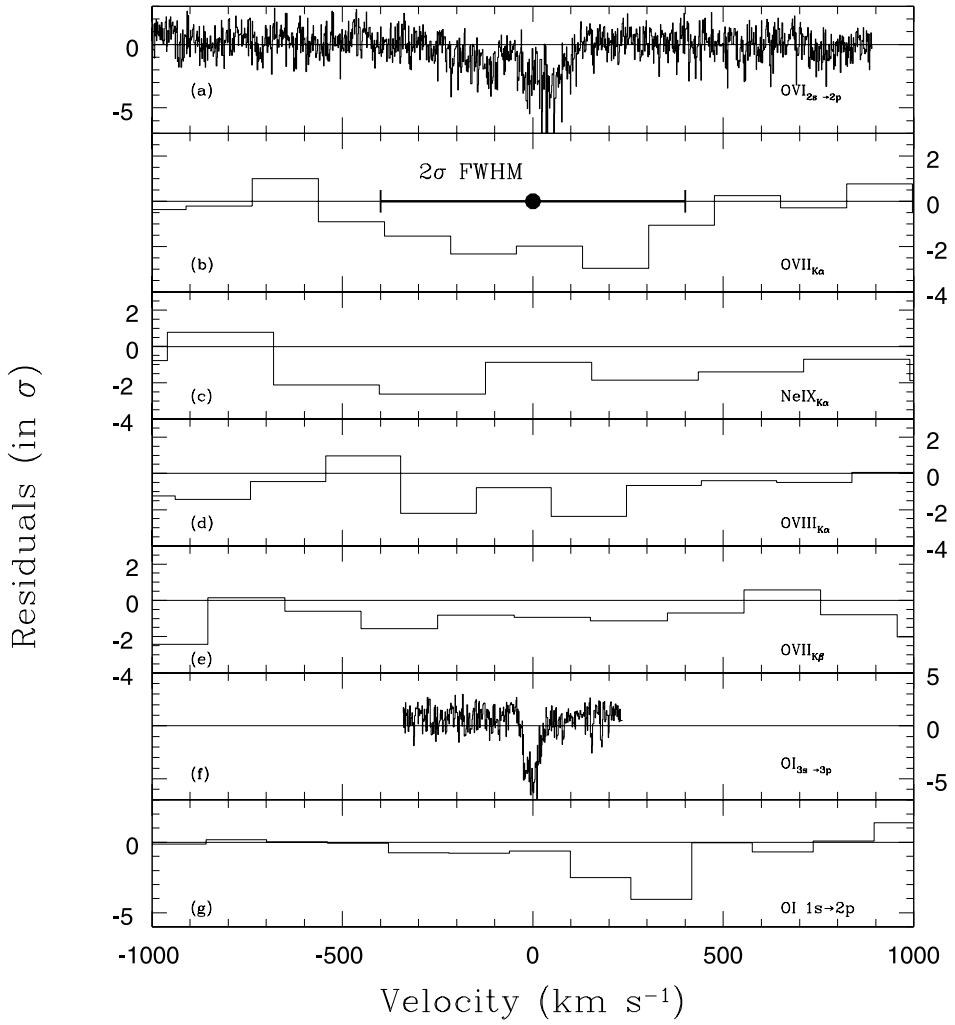

FIG. 3.—Residuals, in velocity space, of the relevant portions of the *FUSE* (*a, f*) and HRCS/LETG (*b, c, d, e, g*) spectra of PKS 2155−304, to their best-fitting continuum models. The residuals are centered, from top to bottom, on the rest-frame wavelengths of the resonant transitions: O VI $2s\rightarrow 2p$, O VII Kα, Ne IX Kα, O VIII Kα, O VII Kβ, O I($\lambda = 23.489$). Bin widths are as follows: (*a, f*) *FUSE*: 2 km s^{-1}; (*b, d, e*) *Chandra*: 190 km s^{-1}; (*g*) *Chandra*: 160 km s^{-1}; (*c*) *Chandra*: 280 km s^{-1}.

absorption (Nicastro, Fiore, & Matt 1999a) to produce COGs for the O VI $2s\rightarrow 2p$ ($\lambda = 1031.9261$), the O VII Kα, the O VIII Kα doublet, and the Ne IX Kα. We assume a Doppler parameter of $b = 200$ km s^{-1}, since this is the observed σ of the O VI $2s\rightarrow 2p$ complex.[10] The COGs are plotted in Figure 4, along with the maximum possible measured EWs (best fit + 2 σ) of each line (EWs are plotted in absolute value). For the O VI $2s\rightarrow 2p$ ($\lambda = 1031.9261$) complex we considered the total EW from the two best-fit Gaussians. All the lines EWs fall well within the linear branches of their COGs. Hence, the lines are not saturated, and the resulting column densities, listed in Table 1, should be reliable.[11]

4. DISCUSSION

The *FUSE* and *Chandra* spectra of PKS 2155−304 contain absorption features from local intervening ionized gas that span a broad ionization interval, from neutral (O I), through mildly ionized (O VI, O VII), to highly ionized (O VII, O VIII, and Ne IX). The neutral and the ionized components have very different dynamical and physical properties and so must belong to two different, spatially separated, systems. The profile of the O VI complex in the *FUSE* spectrum suggests that the ionized component is also made up of at least two different absorbers: one slow-moving, with relatively low internal dispersion velocity and possibly associated with a cloud in the Galactic disk, and one moving toward us with a velocity of about 150 km s^{-1} ($\sim$100 km s^{-1} transforming from the heliocentric to the Galactic standard of rest frame)[12] and with a similar internal dispersion velocity and possibly associated either with an ionized high-velocity cloud in the Galactic halo, or with a WHIM filament.

[10] The broadening due to thermal velocity in a collisionally ionized gas containing a sizeable fraction of O VI would be on the order of 35 km s^{-1} in the single O VI component. Therefore, the assumption here is that some turbulent motion of the gas is producing a dispersion velocity along the line of sight on the order of $\sim$100–200 km s^{-1}.

[11] The partial covering and scattering effects that can occur when the absorbing material is close to the source, as in AGN "warm absorbers" and broad absorption lines (e.g., Arav et al. 2001) do not apply in this case, since PKS 2155−304 has $z = 0.116$, while the absorbers are at their rest wavelengths and so are physically well separated.

[12] See http://nedwww.ipac.caltech.edu/forms/vel_correction.html.

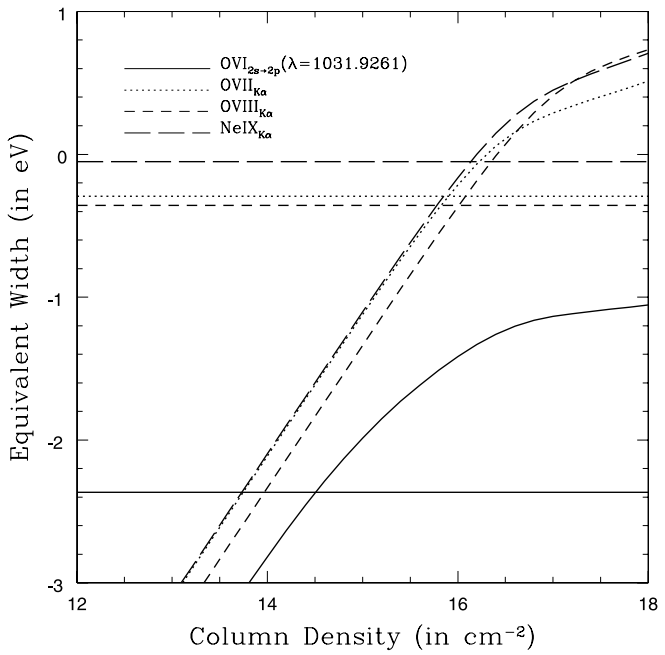

FIG. 4.—COGs for the detected UV and X-ray absorption lines O VI $2s\rightarrow2p$ ($\lambda = 1031.9261$), O VII Kα, O VIII Kα (doublet), and Ne IX Kα. A doppler parameter of $b = 200$ km s^{-1} (the observed σ of the O VI $2s\rightarrow2p$ complex) is assumed. Horizontal solid lines are the maximum possible observed EWs (best fit + 2 σ).

In the next sections we demonstrate that neither pure collisional ionization nor pure photoionization models can account for the presence of strong O VII and Ne IX absorption with the observed intensity of the O VI lines, unless the three absorbers (one X-ray and the two UV) are associated with three different Galactic clouds with drastically different equilibrium conditions (with temperatures differing by an order of magnitude) and thus locations. Alternatively, we show that if there is one highly tenuous absorber, then the photoionization contribution by the diffuse X-ray background (XRB) becomes important and can change the internal ion abundance distribution to account for all the UV and X-ray observational constraints in a single absorbing medium. These solutions, however, imply path lengths on the order of several megaparsecs and so definitively locate the UV-X-ray absorber in the intergalactic medium (IGM), beyond our Galaxy on a scale of the Local Group or somewhat bigger.

4.1. *The XRB Contribution*

For the photoionization contribution by the diffuse, extragalactic X-ray background, we adopt an EUV to gamma-ray spectral energy distribution [SED; i.e., the specific flux $F_{\rm bkg}(E)$] given by a broken power law with an exponential high-energy cutoff [i.e., $F_{\rm bkg}(E) = [K1(E)^{-\alpha_{\rm soft}} + K2(E)^{-\alpha_{\rm hard}}]e^{-(E/E_f)}$, with $K1 = 0$ for $E > E_b$, $K2 = 0$ for $E < E_b$, $\alpha_{\rm soft} = 1.1$, $\alpha_{\rm hard} = 0.4$, $E_b = 0.7$ keV, and $E_f = 50$ keV; we also adopt a low-energy cutoff at energies lower than the hydrogen ionization threshold $E_{\rm H\,I}$]. We assume a normalization of 10 photons s^{-1} cm^{-2} keV^{-1} sr^{-1}, at 1 keV (Parmar et al. 1999; Boldt 1987; Fabian & Barcons 1992). Following the Hellsten et al. (1998) parameterization for the redshift evolution of the X-ray background, we can write the ratio between the diffuse background ionizing photons density and the electron density of a filaments at redshift z (i.e., the ionization parameter U) as

$$U = \left[(1+z)^3/4\pi c\right] n_e^{-1} \int_{\nu_{\rm H\,I}}^{+\infty} d\nu 4\pi \left[F_{\rm bkg}(\nu)/h\nu\right] \simeq 1.4 \times 10^{-7} n_e^{-1} (1+z)^3 = 0.7\delta^{-1}(\Omega_b h^2/0.02)^{-1}\ , \quad (1)$$

where $\nu_{\rm H\,I}$ is the frequency of the H ionization threshold.

In equation (1) we defined the local IGM overdensity compared with the mean density of the universe, $\overline{n_e}$, as $\delta = n_e/\overline{n_e}$, where $\overline{n_e} = [2 \times 10^{-7}(1+z)^3(\Omega_b h^2/0.02)]$ cm^{-3} (Hellsten et al. 1998). Hence, for typical overdensities of $\delta = 10$ (Hellsten et al. 1998; Davé et al. 2001), we expect, at any redshift, $U \sim 0.1\delta_{10}^{-1}$, for $\Omega_b h^2 = 0.0125$ (Walker et al. 1991; $h = 0.5$). Given the flat X-ray spectrum of the X-ray background, XRB photoionization greatly modifies the ionic distribution of a purely collisionally ionized gas at temperatures lower than $\log T \sim 6.4$ for electron densities of $n_e \lesssim 10^{-4}$ cm^{-3} ($\delta \lesssim 800$). Photoionization is not important at typical ISM densities of 10^{-2} to 1 cm^{-3} (e.g., Spitzer 1990; but see § 4.5 for alternative ionizing sources).

4.2. *Models*

We ran CLOUDY (version 90.04; Ferland 1997) to build models for temperatures (in kelvins) from $\log T = 5.1$–8 and densities $n_e = 10^{-7}$ to 1 cm^{-3}. Figure 5 shows the ratios between the predicted ionic abundances of O VII/O VI (*black curves*), O VIII/O VI (*green curves*), O VIII/O VII (*red curves*), and Ne IX/O VII (*blue curves*). Solid curves are for $n_e = 1$ cm^{-3}, while long-dashed curves correspond to $n_e = 10^{-6}$ cm^{-3} (i.e., $\delta \sim 10$). The thick sections of the lines delimit the 2 σ allowed intervals given the measured relative ion column densities derived from the corresponding EWs (see Table 1), using the formula—valid only when the lines are not saturated—$\mathrm{EW}(X^i) \propto A(X) n_{X^i}$ (Nicastro et al. 1999a), where $A(X)$ is the relative abundance of the element X, compared to H, and n_{X^i} is the relative density of the ion i of the element X. Figure 5 uses the total measured EW for the O VI $2s\rightarrow2p$ complex (i.e., narrow and broad components combined).

According to the above formula, the ratio between equivalent widths of two lines from two different ions of the same element then depends only on the ratio of the corresponding equivalent widths. Instead, for ions from different elements, the relative ion densities are proportional to the inverse of their relative metallicity (i.e., $n_{X^i}/n_{Y^j} \propto [EW(X^i)/EW(Y^j)]\,[A(X)/A(Y)]^{-1}$). For the Ne IX/O VII ratio (*blue lines*) we show allowed regions for a solar Ne/O ratio (*magenta dotted line, delimited by perpendicular tick marks*) and for 2.5 times solar ($[\mathrm{Ne/O}]_\odot = 0.158$; Grevesse & Anders 1989; Grevesse & Noels 1993; *blue dashed line*). These values are discussed in § 4.3.

4.3. *Galactic versus Extragalactic Origin*

Let us consider first the Galactic "high-density" solutions, for which the gas is in pure collisional ionization equilibrium. The ratio of O VII Kα to the entire O VI $2s\rightarrow2p$ UV complex (Fig. 5, *thick black curve*) sets a quite stringent upper limit of $\log T \lesssim 5.7$ (T in kelvins) on the allowed temperature of the O VI-O VII absorber, if both the lines are produced by the same material. However, the O VIII and Ne IX ions are clearly too highly populated to be consistent with the intensities of the O VI and O VII lines, requiring

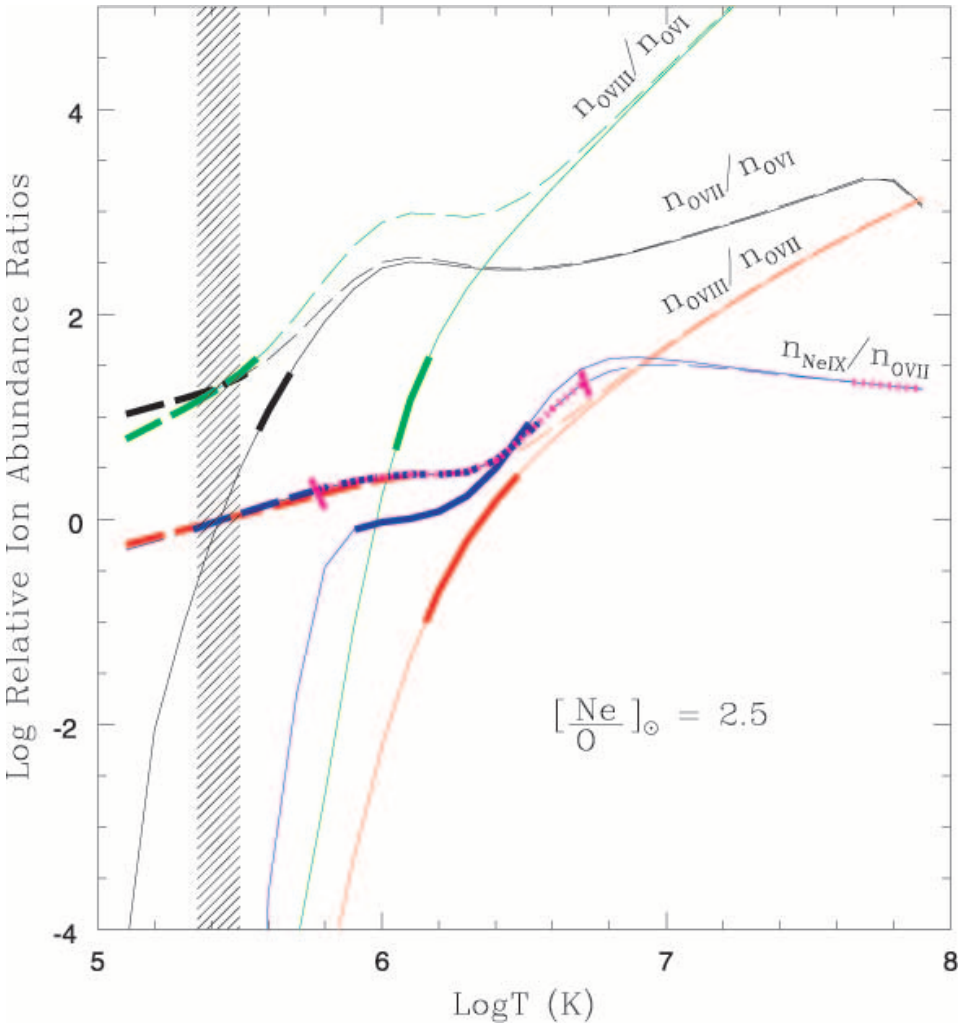

FIG. 5.—Ratios between the predicted ionic abundances of O VII/O VI (*black curves*), O VIII/O VI (*green curves*), O VIII/O VII (*red curves*) and Ne IX/O VII (*blue curves*), for two electron densities: (*a*) $n_e = 1$ cm^{-3} (*solid curves*) and (*b*) $n_e = 10^{-6}$ cm^{-3} (*long-dashed curves*). Thick tracks on these curves delimit the 2 σ allowed intervals for the measured relative abundances ratios for the same ions, derived for the total measured EW of the O VI $2s\rightarrow2p$ complex. Ne/O ratios of 1 (*magenta dotted line*) and 2.5 (*blue dashed line*) times solar are plotted.

$\log T > 6.1$, and so no common solution exists for all the lines. We find that this is true for any $n_e \gtrsim 10^{-2}$ cm^{-3}.

Let us now consider the extreme extragalactic "low-density" ($n_e = 10^{-6}$ cm^{-3}) solution (Fig. 5, *thick long-dashed curves*), where photoionization by the diffuse XRB overionizes the medium. These conditions allow the O VI, O VII, and O VIII ions to have a common temperature (Fig. 5, *shaded region*) for the relatively low temperature range $5.35 \leq \log T \leq 5.50$. A consistent solution for even the oxygen lines requires the absorber to be highly tenuous ($n_e \lesssim 5 \times 10^{-6}$ cm^{-3}). A solar Ne/O ratio (*magenta dots*) is not consistent with these conditions, but an Ne/O ratio of $\sim$2.5 times solar (*blue dashes*) provides consistency for all the ions (see § 4.7). Increasing the Ne/O metallicity ratio decreases the Ne IX/O VII relative density ratio estimated from the corresponding measured EW ratio (see § 4.2) and so lets the thick intervals in Figure 5 shift toward the left on the theoretical $n_{\rm Ne\,IX}/n_{\rm O\,VII}$ curve, down to the region where a common solution for all the ions can be found.

For a given temperature, we can derive the equivalent H column density of this gas. Assuming Ne/O = 2.5 and $\log T = 5.45$ gives $N_{\rm H} \simeq 1.5 \times 10^{19}[{\rm O/H}]_\odot^{-1}$ cm^{-2}. This translates, for a constant electron density of $n_e = 10^{-6}$ cm^{-3}, to a linear size of the absorbing cloud of gas of $4.9[{\rm O/H}]_\odot^{-1}$ Mpc, consistent with a filament with an overdensity of $\sim$10 located in the intergalactic medium near to our Galaxy. For O abundances of 0.3 times solar (as found in clusters of galaxies; Sarazin 1988), the size would increase to $\sim$15 Mpc ($\sim$2% of the distance to PKS 2155−304, and $\sim$25% of the distance to the first group of galaxies close to our line of sight to the blazar; Penton, Stocke, & Shull 2000).

4.4. *Multicomponent Solutions*

The preceding discussion is based on the hypothesis that both the broad and narrow components of the O VI absorption complex are produced by a single, structured absorber that is also producing the X-ray absorption. Here we explore alternative multicomponent solutions.

Let us suppose that only one of the two O VI $2s\rightarrow2p$ absorption lines in the UV spectrum is associated with the X-ray absorber. The broader O VI line contributes about $\frac{1}{3}$ to the total observed equivalent width from the O VI system,

while the remaining $\frac{2}{3}$ are provided by the narrower line (see Table 1). Based on the strengths of the O VI $2s\rightarrow2p$ lines and on the above discussion, it is then natural to associate the broader UV component with the X-ray absorber. In this case the narrow and more intense O VI component would be produced by a Galactic cloud of moderately ionized gas in collisional equilibrium. This "narrow" line gas must have a temperature of $\log T^{\rm narrow} \gtrsim 5.0$ if the size of the cloud is not to exceed 1 kpc, the size of a big halo cloud (e.g., Spitzer 1990), given the measured EW and assuming a maximum Galactic ISM density of $\sim$1 cm^{-3}. The upper limit on the temperature is instead set by the observed EW [narrow O VI ($2s\rightarrow2p$)] /EW(O VII Kα) ratio, and this gives $\log T^{\rm narrow} \ll 5.6$.

The second absorber should instead produce the broader and weaker O VI line, and all the X-ray lines. We tested this hypothesis by building a diagram similar to that in Figure 5 but considering a variable fraction (from 0 to 1) of the EW of the broad O VI $2s\rightarrow2p$ line (Fig. 6).We find that equilibrium, high-density solutions exist only if a fraction of 5%–25% (at 2 σ) of the broad O VI line is produced by the same gas producing the X-ray absorption. These solutions are limited to a range of temperatures around $\log T = 6.4$, whose width depends on the relative [Ne/O] abundance: $\Delta(\log T) = 0.16$–0.32 for $[{\rm Ne/O}]_\odot = 1$–2 (Fig. 6, *hatched regions*). For $\log T = 6.4$ and $[{\rm Ne/O}]_\odot = 1$, we find $N_{\rm H} = 2.2 \times 10^{19}[{\rm O/H}]_\odot^{-1}$ and thus a linear size of $D = 7[{\rm O/H}]_\odot^{-1}$ pc, for $n_e = 1$ cm^{-3}.

Since only 25% of the broad O VI $2s\rightarrow2p$ can come from X-ray–absorbing gas, a third ad hoc Galactic absorber similar in dynamical properties to the absorber imprinting the broad O VI $2s\rightarrow2p$ line, but with temperature differing by at least an order of magnitude from the temperature of the UV-X-ray absorber, is required to explain the remaining broad O VI absorption. Alternatively, a highly structured and, again, ad hoc multitemperature plasma, with at least two zones separated by a sharp front and with the same kinematics, would be needed to account for all the observed UV and X-ray lines. We can broaden the range of allowed temperature and increase the fraction of O VI absorption produced by the X-ray absorber by allowing both the Ne/O ratio to be supersolar and the gas density to be lower than $\sim10^{-4}$ cm^{-3}. However, this converges to the extragalactic solution (§ 4.3). We find that an acceptable solution with a minimum size is obtained for $\log T = 5.7$, $n_e = 6 \times 10^{-6}$ (i.e., $\delta \sim 60$), and Ne/O = 2, which gives $N_{\rm H} = 6 \times 10^{19}[{\rm O/H}]_{0.3\odot}^{-1}$ cm^{-2} and $D = 3[{\rm O/H}]_{0.3\odot}^{-1}$ Mpc.

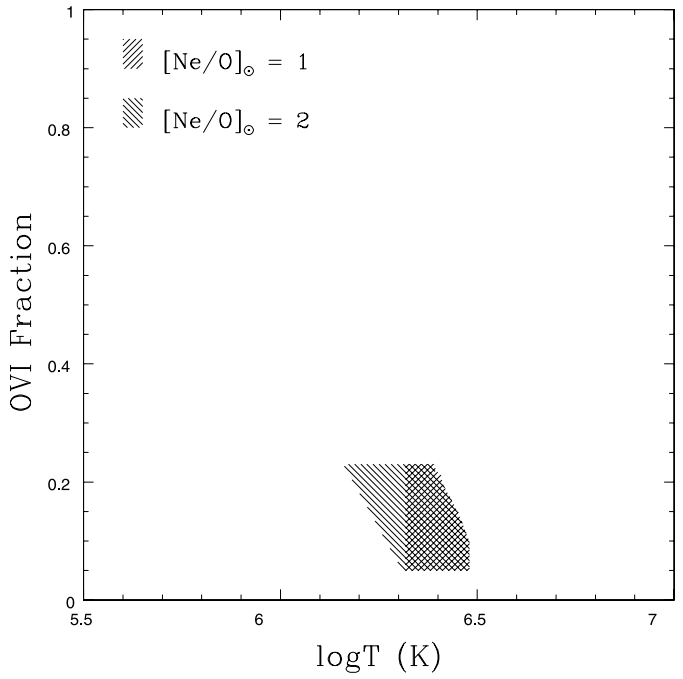

FIG. 6.—Fraction of broad O VI line [f(O VI)] produced by the same gas producing the X-ray absorption, as a function of gas temperature. The diagram shows the two regions (for $[{\rm Ne/O}]_\odot = 1$ [*crosshatched region*], and $[{\rm Ne/O}]_\odot = 2$ [*hatched region*]), in the f(O VI)–log T space, for which common UV–X-ray Galactic solutions do exist; at most 25% of the broad O VI $2s\rightarrow2p$ can come from a Galactic cloud of X-ray–absorbing gas

4.5. *Alternative Photoionizing Sources*

As we have demonstrated (§§ 4.1 and 4.3), X-ray photoionization is needed to modify the ion relative abundance distribution from the pure collisionally ionized case (with $\log T = 5.3$–5.7) to allow for the simultaneous presence of O VI, O VII, and O VIII, and also Ne IX. In order for the photoionization contribution to play a significant role, the ionization parameter has to be on the order of $U \sim 0.1$ (§ 4.1). Since the ionization parameter U is simply the ratio between the number density of ionizing photons and the electron density of the gas, U increases as either the electron density in the gas decreases (as in the IGM case) or the distance between the source of ionizing photons and the gas cloud decreases. So high values of U might also be reached in gas with typical ISM densities (i.e., $n_e \sim 10^{-2}$ to 1 cm^{-3}) illuminated by other, discrete and locally much brighter hard X-ray sources than the XRB. In this section we explore this second possibility.

4.5.1. *Isotropic Nearby Source*

On the basis of the needed value of $U \sim 0.1$ we can put constraints on the brightness of the ionizing source as seen by us, and on the angular separation between the source and the gas cloud. Let us consider an intervening cloud of gas located at a distance r from us, along a given line of sight, and an ionizing source, located at a distance D from us. Let d be the distance between the ionizing source and the gas cloud. We can write (1) $L = 4\pi D^2 F_{\rm obs}$, (2) $L = 4\pi d^2 F_{\rm ion}$, and (3) $rtg\theta = d$. In the above equations, L is the source luminosity, and $F_{\rm obs}$ and $F_{\rm ion}$ are the source fluxes as seen by us and the gas cloud, respectively. These two fluxes are related to each other through the source-gas angular separation θ: $F_{\rm ion} = (\sin\theta)^{-2} F_{\rm obs}$. The ionization parameter U at the illuminated face of the cloud can then be written as a function of the source flux as seen by us: $U = qn_e^{-1}c^{-1}(\sin\theta)^{-2}$, where $q = \int_{E_{\rm H}}^{+\infty} dE E^{-1} f_{\rm obs}(E)$ is the total flux of ionizing photons [$F_{\rm obs} = \int dE f_{\rm obs}(E)$]. To maximize the contribution from hard X-ray ionizing photons we use as the ionizing continuum a cutoff power law with $\Gamma = 1.5$ from the H-ionization threshold up to 100 keV, and $\Gamma = 4$ from 100 keV up to infinity. This gives a total flux of ionizing photons of $q \simeq 1.3 \times 10^9 F_{\rm obs}^{2-10}$ photons s^{-1} (where $F_{\rm obs}^{2-10}$ is the observed flux between 2 and 10 keV, and we assumed $F_{\rm obs} = 3 \times F_{\rm obs}^{2-10}$). Our value $U \sim 0.1$ then gives $U \simeq 4 \times 10^{-2} n_e^{-1} (F_{\rm obs}^{2-10})_{\rm CGS} (\sin^{-2}\theta) \sim 0.1$. For $\theta = 30'$ and gas densities in the ISM range $n_e = 10^{-2}$ to 1 cm^{-3}, then, the 2–10 keV observed flux must be as large as $F_{\rm obs}^{2-10} \sim 2 \times (10^{-6}$ to $10^{-4})$ ergs s^{-1} cm^{-2} ($\sim10^2$–10^4 crab),

to efficiently ionize the gas. For a 30 times smaller separation, this fluxes reduce to $2 \times (10^{-9}$ to $10^{-7})$ ergs s^{-1} cm^{-2} ($\sim$0.1–10 crab). No such source is currently seen.

For halo distances of 30 kpc the implied 2–10 keV luminosities are $L_{\rm obs}^{2-10}(\theta = 30') = 2 \times (10^{41}$–$10^{43})$ ergs s^{-1} ($d = 260$ pc), far too large for any known stellar-size Galactic source, and $L_{\rm obs}^{2-10}(\theta = 1') = 2 \times (10^{38}$–$10^{40})$ ergs s^{-1} ($d = 8$ pc), just about the maximum observed luminosity for the most luminous known ultraluminous-X-ray sources (ULXs) or beamed microquasars. For the much closer distances of Galactic disk objects, say, 10 pc, these luminosities reduce to more normal values for X-ray binaries [i.e., $L_{\rm obs}^{2-10}(\theta = 30') = 2 \times (10^{34}$–$10^{36})$ ergs s^{-1}, and $L_{\rm obs}^{2-10}(\theta = 1') = 2 \times (10^{31}$–$10^{33})$ ergs s^{-1}] but the physical separations between the source and the gas cloud become very small: $d = 0.09$ pc and $d = 0.003$ pc, respectively. So, either very luminous sources, or very close source-to-gas systems are needed to efficiently ionize a tenuous gas cloud in our Galaxy to the observed degree.

We searched the *ROSAT*-WGACAT (White, Giommi, & Angelini 1994) for bright X-ray sources in a 30′ radius cylinder, centered on the line of sight to PKS 2155−304. We found 33 unidentified sources plus an F0 star with *ROSAT*-PSPC count rates between 0.0019 and 0.024 counts s^{-1}, and angular distances from the line of sight from $\theta = 2\farcm1$ to $\theta = 20\farcm4$. The closest of these sources to the PKS 2155−304 line of sight has a count rate of 0.0073 (source A: 1WGA J2158.8−3011), while the brightest (0.025 counts s^{-1}) is at a distance of 15′.1 (source B: 1WGA J2158.2−3000). We used PIMMS[13] to convert these count rates into flux. To maximize the possible contribution at energies $E > 1$ keV, we assumed a hard X-ray continuum (a power law with $\Gamma = 1.5$) heavily absorbed by a column of $N_{\rm H} = 10^{22}$ cm^{-2} intrinsic neutral gas. This gave 2–10 keV fluxes of 10^{-12} ergs s^{-1} cm^{-2} (5×10^{-5} crab), for source A, and 3.6×10^{-12} ergs s^{-1} cm^{-2} (1.8×10^{-4} crab) for source B, at least (i.e., using $n_e = 10^{-2}$ cm^{-3}) 4 and 5 orders of magnitude, respectively, lower than the values required to photoionize the gas at these angular separations.

4.5.2. *Beamed Nearby Source*

Let us consider a microquasar highly beamed into the direction of the gas cloud and whose line of sight to us is somewhat perpendicular to the beam direction. The probability for a microquasar to be beamed in the direction of the gas cloud, and located within a 20–130 pc radius sphere from the gas cloud, depends on the distribution of the parent population, which, for microquasars, is largely unknown. We can compute here the minimum beaming factor needed, in the above optimal geometrical configuration, for source A or B to efficiently ionize a cloud of gas along the line of sight to PKS 2155−304. The luminosity amplification due to beaming, in the direction of the jet, is given by $L_{\rm beam} = L_{\rm intr}(2\gamma)^p$. The observed luminosity along a perpendicular direction is instead deboosted by the factor $L_{\rm obs} = L_{\rm intr}\gamma^{-p}$ (Urry & Shafer 1984). In the above equations, $L_{\rm intr}$ is the source intrinsic luminosity, γ is the Lorentzian factor, and $p \simeq 4$ (Urry & Shafer 1984). Solving for the intrinsic luminosity, and using as maximum value for the beamed luminosity of a microquasar $L_{\rm beam} = 5 \times 10^{40}$ ergs s^{-1} and the observed value of $L_{\rm obs} = 4 \times 10^{35}$ ergs s^{-1} (for source B, at 30 kpc), we obtain a minimum relativistic factor of $\gamma \geq 3$, to compare with the estimated upper limit of $\gamma = 3$ for the microquasar GRS 1915+105 (Mirabel & Rodriguez, 1999). Any deviation from the above ideal geometry would give a much larger Lorentz factor.

4.5.3. *Historical Nearby Source*

Low-density gas has long recombination times. A source may thus have been much more luminous in the past and ionized the gas then, from which the gas has not yet recovered. Let us first suppose that the most luminous X-ray source we are currently seeing in the *ROSAT* archive is a binary system that went through a ULX phase (King et al. 2001) in the past [from the calculation in § 4.5.1, for sources A and B we need $L(\text{outburst})/L(\text{now}) > 10^4$–$10^5$, respectively].[14] The recombination time for the O VII-O VIII ions in gas with electron density of $n_e = 1$ cm^{-3} is of about $t_{\rm rec} \sim 10^5$ yr (Nicastro et al. 1999b). Typical ULX phases are thought to last for $\sim 10^5$ yr, and in our Galaxy the total estimated rate of ULXs is of 1 every 10^5 yr (King et al. 2001). So, allowing for a maximum delay of $t_{\rm delay} = t_{\rm rec} = 10^5$ yr, we may expect $N = 2$ ULXs in all the Galaxy over a period of $\Delta t = t_{\rm phase} + t_{\rm delay} = 2 \times 10^5$ yr. Assuming for the halo a 30 kpc radius sphere, this gives a ULX density, over the same period, of $n = 2/[(4/3)\pi \times (30)^3$ kpc$] \simeq 1.8 \times 10^{-5}$ kpc^{-3}. So the maximum number of ULXs expected over a period Δt in a random $R_{\rm max} = 20$–130 pc radius sphere in our Galaxy (the physical distances between sources A and B and the line of sight to PKS 2155−304, if both sources are put at 30 kpc from us, in the outskirts of the Galactic halo) is of $N_{\rm max} = 6 \times 10^{-10}$ to 2×10^{-7}, making prior ionization by a powerful transient source highly unlikely, albeit with a posteriori statistics.

4.5.4. *Historical AGN at Galactic Center*

A final possibility is that in the past the center of our Galaxy went through an active galactic nucleus (AGN) phase, producing far higher luminosities and photoionizing any low-density ($n_e \sim 10^{-2}$ cm^{-3}) clouds in the Galactic halo. At these densities we have $t_{\rm rec}$(O VII, O VIII) $\sim 10^7$ yr. Let us then suppose that less than 10^7 yr ago the 2×10^6 $M_\odot$ black hole in the center of our Galaxy (Chakrabarty & Saha 2001) was emitting at its Eddington luminosity of 2×10^{44} ergs s^{-1}. Assuming a typical SED for AGNs (Mathews & Ferland 1987) this would produce an ionization parameter of $U_{\rm AGN} = 2.4 \times 10^{45} \times D^{-2}$ at the surface of $n_e = 10^{-2}$ cm^{-2} halo clouds located at a distance D from the central AGN. To produce the observed line ratios, the photoionization contribution must be such that $U_{\rm AGN} \sim 0.1$ at the illuminated face of such a cloud of gas. This gives a distance for the gas cloud of $D \sim 36$ kpc, consistent with the outermost size of the Galactic halo. This solution requires that all halo clouds would show UV and X-ray absorption with similar physical properties as those observed in PKS 2155−304. Using the much lower luminosities estimated by *ASCA* for the central AGN in our Galaxy about 10^4 yr ago (i.e., $L \sim 10^{41}$–10^{42} ergs s^{-1}; Koyama et al. 1996), gives distances of 1–5 kpc, well within the Galaxy's halo, and therefore not consistent with the galactic coordinates of PKS 2155−304

[13] See http://legacy.gsfc.nasa.gov/Tools/w3pimms.html.

[14] Such outbursts have been observed in X-ray novae between quiescent and active phases (e.g., Narayan, Garcia, & McClintock 2002).

(given our distance of about 10 kpc from the Galactic center).

4.6. *Properties of the WHIM Gas*

From our analysis of the combined UV and X-ray data, we conclude that the X-ray absorption and at least the broad O VI $2s\rightarrow2p$ are likely to be produced in tenuous extragalactic medium, with $n_e \sim 6 \times 10^{-6}$ cm^{-3}. From the position of the broad O VI ($2s\rightarrow2p$) and assuming that the feature lies within a few Mpc from our Galaxy, the gas is falling toward our Galaxy with a bulk velocity of $\sim$100 km s^{-1} (in the Galactic standard of rest frame). The feature has a dispersion velocity ($\sim$300 km s^{-1}) comparable with the bulk velocity and a temperature of $\log T \sim 5.7$. The implied overdensity is $\delta \sim 60$, and the total linear size of the feature along our line of sight is about $3\delta_{60}^{-1}[\mathrm{O/H}]_{0.3\odot}^{-1}$ Mpc.

The Ne/O abundance can be reduced to solar if we allow for inhomogeneities in the flow, since inhomogeneities increase the upper limits on both the temperature and the density, and so also decrease the lower limit on the linear size of the feature (from 3 $[\mathrm{O/H}]_{0.3\odot}^{-1}$ Mpc to few $\times\, 10^2[\mathrm{O/H}]_{0.3\odot}^{-1}$ kpc). Such inhomogeneities may arise near our Galaxy halo, where the gas may mix with denser medium, cooling and producing part of the observed broad O VI $2s\rightarrow2p$ absorption.

The above overdensities and linear sizes are consistent with those predicted for the WHIM by hydrodynamic simulations for the formation of structure in the local universe (e.g., Hellsten et al. 1998), and in particular in our Local Group (Kravtsov, Klypin, & Hoffman 2001). According to these simulations, the local IGM is concentrated in filaments with overdensities of $\delta \sim 5$–100 connecting already virialized structured (galaxies and clusters of galaxies) that were shock-heated during the collapse of the density perturbations. The average sizes of these perturbations are on the order of 30–50 Mpc in the local universe, but the total extent of the density peaks are usually not larger than a few Mpc. The velocities of the matter in these filaments should be on the order of the proper motions of the virialized structures that they connect, $\sim$100–200 km s^{-1}. We note that these velocities are of the same order as those observed on the blue side of the structured and complex O VI $2s\rightarrow2p$ profile in the UV spectrum of PKS 2155$-$304.

We also note that both the dynamics of this gas (as derived from the O VI line) and its physical state are very similar to those found (using UV absorption lines only) for the intervening ionized absorber along the line of sight to the quasar H1821+643 (Tripp et al. 2001): internal dispersion velocities on the order of $\sim$150 km s^{-1} (FWHM of the broad Lyα line), temperature in the range $5.3 < \log T < 5.6$ (assuming pure collisional ionization), and path length of about 3 Mpc (using $H_0 = 50$ km s^{-1} Mpc^{-1}). We predict that the planned high-resolution and high-quality X-ray spectra of this object should then show O VII Kα absorption with an intensity similar to that found here.

4.7. *The* Ne/O *Problem: Dust Depletion*

In virtually all the cases discussed, the Ne/O ratio in the absorber along the line of sight toward PKS 2155$-$304 is required to be higher than solar. There are various ways to reconcile with this problem:

1. Type II supernovae give rise to Ne/O ratios much higher than Type I supernovae, compared to Si (Tsuro et al. 1997 and references therein).
2. O can be depleted on to dust grains, but a noble gas like Ne would not. If superwinds from galaxies are responsible for the enrichment of the IGM, then in order to produce high gaseous Ne/O ratios compared to solar, they must be able to produce a considerable amount of dust before leaving the high-density galaxy environment.
3. In the modeling above, we have assumed a simple parameterization of ionizing background. The true shape of the background is clearly more complex, and a harder background would result in a large Ne/O ratio. Any or all of these factors might be playing a role in the observed value of [Ne/O].

It is important to notice that dust can easily survive at the kinetic temperatures (i.e., few $\times\, 10^5$ K) and densities (i.e., $n_e \sim$ few $\times\, 10^{-6}$ cm^{-3}) of such a warm IGM filament. In such a regime, the sputtering lifetime is inversely proportional to the gas density and largely independent from the dust grain composition and gas temperature (Draine & Salpeter 1979a, 1979b). The survival time of a small interstellar grain of size $\sim$0.01 μm will be larger than 10^{10} yr in the IGM filament and even larger for grains of larger size. We estimated the reddening expected along the line of sight to PKS 2155$-$304, based on (1) the observed equivalent H column density, (2) the typical size of a silicate dust grain, and (3) a typical ISM gas/dust ratio. In this condition the estimated $E(B-V)$ is of about 2×10^{-2} mag, fully consistent with the observations (Schlegel, Finkbeiner, & Davis1998).

Finally, we note that [Ne/O] overabundances of $\sim$2–3, compared to solar, have already been observed in several astrophysical environments (e.g., Paerels et al. 2001; Brinkman et al. 2001), strongly suggesting that the non–O-depleted values of this quantity, measured in stellar atmospheres, are not representative of the average gaseous [Ne/O] ratio in the universe.

5. CONCLUSIONS

In this paper we report the first discovery of the X-ray forest of absorption lines produced by highly ionized intergalactic medium. High-significance X-ray absorption lines of O VII, O VIII, and Ne IX are detected along the line of sight to the bright blazar PKS 2155$-$304 and are associated with a known O VI UV absorber. We demonstrate that the dynamical properties of the X-ray and the UV absorber are fully consistent with each other and that a reasonable common and self-consistent physical solution can be found only if photoionization and collisional ionization both contribute to the ionization of the absorbing gas. This requires electron densities of about 6×10^{-6} cm^{-3} for the diffuse X-ray background to be significant. This low density requires a linear size, along the line of sight, on the order of $3[\mathrm{O/H}]_{0.3\odot}^{-1}$ Mpc. This clearly locates the absorber outside our Galaxy in intergalactic space. We demonstrate that both the dynamical and physical properties of such an absorber are remarkably consistent with those predicted for the low-redshift warm phase of the IGM as predicted by hydrodynamic simulations for the formation of structures in the universe. Finally, we find that solutions with a Ne/O ratio of about 2.5 times solar are favored, suggesting Type II supernova enrichment, or the presence of dust in the IGM.

This work has been partly supported by the NASA grant ADP NAG-5-10814 (F. N.), the *Chandra* grant DDO-1005X (F. N. and A. F.), CXC grant NAS8-39073 (F. N. and A. F.) and the NASA grant LTSA NAG-5-8913 (S. M.).

REFERENCES

Aldcroft, T., Elvis, M., McDowell, J., & Fiore, F. 1994, ApJ, 437, 584
Arav, N., Brotherton, M. S., Becker, R. H., Gregg, M. D., White, R. L., Price, T., & Hack, W. 2001, ApJ, 546, 140
Boldt, E. 1987, in IAU Symp. 124, Observational Cosmology, ed. A. Hewitt, G. Burbidge, & Li Zhi Fang (Dordrecht: Reidel), 611
Brinkman, A. C., et al. 2000, ApJ, 530, L111
———. 2001, A&A, 365, L324
Chakrabarty, D., & Saha, P. 2001, AJ, 122, 232
Davé, R., et al. 2001, ApJ, 552, 473
Dickey, J. M., & Lockman, F. J. 1990, ARA&A, 28, 215
Draine, B. T., & Salpeter, E. E. 1979a, ApJ, 231, 77
———. 1979b, ApJ, 231, 438
Fabian, A. C., & Barcons, X. 1992, ARA&A, 30, 429
Falomo, R., Pesce, J. E., & Treves, A. 1993, ApJ, 411, L63
Fang, T., & Canizares, C. R. 2000, ApJ, 539, 532
Ferland, G. J. 1997, HAZY: A Brief Introduction to CLOUDY (Lexington: Univ. Kentucy Phys. Dept. Int. Rep.)
Fiore, F., Nicastro, F., Savaglio, S., Stella, L., & Vietri, M. 2000, ApJ, 544, L7
Grevesse, N., & Anders, E. 1989, in AIP Conf. Proc. 183, Cosmic Abundance of Matter, ed. C. J. Waddington (New York: AIP), 1
Grevesse, N., & Noels, A. 1993, in Origin and Evolution of Elements, ed. N. Prantzos, E. Vangioni-Flam, & M. Casse (Cambridge: Cambridge Univ. Press), 15
Hellsten, U., Gnedin, N. Y., & Miralda-Escudé, J. 1998, ApJ, 509, 56
Jenkins, E. B. 1978a, ApJ, 219, 845
———. 1978b, ApJ, 220, 107
Kataoka, J., Takahashi, T., Makino, F., Inoue, S., Madejski, G. M., Tashiro, M., Urry, C. M., & Kubo, H. 2000, ApJ, 528, 243
King, A. R., Davies, M. B., Ward, M. J., Fabbiano, G., & Elvis, M. 2001, ApJ, 552, L109
Koyama, K., Maeda, Y., Sonobe, T., Takeshima, T., Tanaka, Y., & Yamauchi, S. 1996, PASJ, 48, 249
Krause, M. O. 1994, Nucl. Instrum. Methods Phys. Res., 87, 178
Kravtsov, A. V., Klypin, A., & Hoffman, Y. 2001, ApJ, submitted (astro-ph/0109077)
Mathews, W. G., & Ferland, G. J. 1987, ApJ, 323, 456
Mirabel, I. F., & Rodriguez, L. F. 1999, ARA&A, 37, 409
Moos, H. W., et al. 2000, ApJ, 538, L1
Narayan, R., Garcia, M. R., & McClintock, J. E. 2002, in Proc. 9th Marcel Grossmann Meeting, ed. V. Gurzadyan, R. Jantzen, & R. Ruffini (Singapore: World Scientific), in press
Nicastro, F., Fiore, F., & Matt, G. 1999a, ApJ, 517, 108
Nicastro, F., Fiore, F., Perola, G. C., & Elvis, M. 1999b, ApJ, 512, 184
Paerels, F., et al. 2001, ApJ, 546, 338
Parmar, A. N., Guainazzi, M., Oosterbroek, T., Orr, A., Favata, F., Lumb, D., & Malizia, A. 1999, A&A, 345, 611
Penton, S. V., Stocke, J. T., & Shull, J. M. 2000, ApJS, 130, 121
Perna, R., & Loeb, A. 1998, ApJ, 503, L135
Sarazin, C. L. 1988, X-Ray Emission from Clusters of Galaxies (Cambridge: Cambridge Univ. Press)
Savage, B. D., et al. 2000, ApJ, 538, L27
Schlegel, D. J., Finkbeiner, D. P., & Davis, M. 1998, ApJ, 500, 525
Sembach, K. R., et al. 2000, ApJ, 538, L31
Spitzer, L. 1978, Physical Processes in the Interstellar Medium (New York: Wiley)
———. 1990, ARA&A, 28, 71
Tripp, T. M., Giroux, M. L., Stocke, J. T., Tumlinson, J., & Oegerle, W. R. 2001, ApJ, 563, 724
Tsuro, T. G., Awaki, H., Koyama, K., & Ptak, A. 1997, PASJ, 49, 619
Urry, C. M., & Shafer, R. A. 1984, ApJ, 280, 569
Verner, D. A., Verner, E. M., & Ferland, G. J. 1996, At. Data Nucl. Data Tables, 64, 1
Walker, T. P., Steigman, G., Kang, H.-S., Schramm, D. M., & Olive, K. A. 1991, ApJ, 376, 51
White, N., Giommi, P., & Angelini, L. 1994, IAU Circ. 6100
York, D. G. 1977, ApJ, 213, 43